Fermi National Accelerator Laboratory

FERMILAB-Pub-99/290-T

A Method for Identifying H $\to \tau\tau \to$ e$\pm\mu\mp$ p$_T$ at the CERN LHC

T. Plehn and D. Zeppenfeld

University of Wisconsin Madison
Madison, Wisconsin 53706

D. Rainwater

Fermi National Accelerator Laboratory
P.O. Box 500, Batavia, Illinois 60510

November 1999

Submitted to *Physical Review D*

Operated by Universities Research Association Inc. under Contract No. DE-AC02-76CH03000 with the United States Department of Energy

Disclaimer

This report was prepared as an account of work sponsored by an agency of the United States Government. Neither the United States Government nor any agency thereof, nor any of their employees, makes any warranty, expressed or implied, or assumes any legal liability or responsibility for the accuracy, completeness, or usefulness of any information, apparatus, product, or process disclosed, or represents that its use would not infringe privately owned rights. Reference herein to any specific commercial product, process, or service by trade name, trademark, manufacturer, or otherwise, does not necessarily constitute or imply its endorsement, recommendation, or favoring by the United States Government or any agency thereof. The views and opinions of authors expressed herein do not necessarily state or reflect those of the United States Government or any agency thereof.

Distribution

Approved for public release; further dissemination unlimited.

Copyright Notification

This manuscript has been authored by Universities Research Association, Inc. under contract No. DE-AC02-76CH03000 with the U.S. Department of Energy. The United States Government and the publisher, by accepting the article for publication, acknowledges that the United States Government retains a nonexclusive, paid-up, irrevocable, worldwide license to publish or reproduce the published form of this manuscript, or allow others to do so, for United States Government Purposes.

University of Wisconsin - Madison

MADPH-99-1142
FERMILAB-Pub-99/290-T
hepph/yymmnnn
November 1999

A method for identifying $\mathbf{H \to \tau\tau \to e^{\pm}\mu^{\mp}\not{p}_T}$ at the CERN LHC

T. Plehn[1], D. Rainwater[2] and D. Zeppenfeld[1]

[1]*Department of Physics, University of Wisconsin, Madison, WI 53706*
[2]*Fermi National Accelerator Laboratory, Batavia, IL 60510*

Abstract

Weak boson fusion promises to be a copious source of intermediate mass Higgs bosons at the LHC. The additional very energetic forward jets in these events provide for powerful background suppression tools. We analyze the subsequent $H \to \tau\tau \to e^{\pm}\mu^{\mp}\not{p}_T$ decay for Higgs boson masses in the 100-150 GeV range. A parton level analysis of the dominant backgrounds demonstrates that this channel allows the observation of $H \to \tau\tau$ in a low-background environment, yielding a significant Higgs boson signal with an integrated luminosity of order 60 fb^{-1} or less, over most of the mass range. We also restate a No-Lose Theorem for observation of at least one of the CP-even neutral Higgs bosons in the MSSM, which requires an integrated luminosity of only 40 fb^{-1}.

I. INTRODUCTION

The search for the Higgs boson and, hence, for the origin of electroweak symmetry breaking and fermion mass generation, remains one of the premier tasks of present and future high energy physics experiments. Fits to precision electroweak (EW) data have for some time suggested a relatively small Higgs boson mass, of order 100 GeV [1], which is also the preferred mass range for the lightest Higgs boson in the minimal supersymmetric extension of the Standard Model (MSSM).

For the intermediate mass range, most of the literature has focused on Higgs boson production via gluon fusion [2] and $t\bar{t}H$ [3] or $WH(ZH)$ [4] associated production. Cross sections for Standard Model (SM) Higgs boson production at the LHC are well-known [2], and while production via gluon fusion has the largest cross section by almost one order of magnitude, there are substantial QCD backgrounds. A search for the very clean four-lepton signature from $H \to ZZ$ decay can find a Higgs boson in the mass region $M_H \gtrsim 125$ GeV, but due to the small branching fraction of this mode very large integrated luminosities, up to 100 fb $^{-1}$ or more, are required. For Higgs boson masses less than about 140 GeV, the inclusive search for $H \to \gamma\gamma$ events is usually considered the most promising strategy [5], while for $140 < M_H < 200$ GeV the most promising search is for decay to W pairs [5–8].

The search for MSSM Higgs bosons must include neutral CP even and CP odd mass eigenstates, as well as charged ones. The upper mass limit of ~ 130 GeV [9,10] on the light scalar makes

it look similar to its intermediate-mass Standard Model analogue, for large regions of the MSSM parameter space. While one would expect the most promising channel to again be $\gamma\gamma$ decay [2,5], the branching ratio for this mode is even smaller than in the Standard Model.

The second largest production cross section is predicted for weak-boson fusion (WBF), $qq \to qqVV \to qqH$. These events contain additional information in their observable quark jets. Techniques like forward jet tagging [11–13] can then be exploited to significantly reduce the backgrounds. WBF and gluon fusion nicely complement each other: together they allow for a measurement of the $t\bar{t}H/WWH$ coupling ratio.

Another feature of the WBF signal is the lack of color exchange between the initial-state quarks. Color coherence between initial- and final-state gluon bremsstrahlung leads to suppressed hadron production in the central region, between the two tagging-jet candidates of the signal [14]. This is in contrast to most background processes, which typically involve color exchange in the t-channel and thus lead to enhanced hadronic activity between the tagging jets. We exploit these features, via a veto of soft jet activity in the central region [15].

We have previously established the feasibility of WBF intermediate-mass Higgs production as both a discovery channel (via $H \to W^{(*)}W^{(*)} \to e^{\pm}\mu^{\mp}\not{p}_T$ decays [6,7]) and as a means to provide the first direct Higgs boson-fermion coupling measurement [16,7] ($H \to \tau\tau \to h^{\pm}\ell^{\mp}\not{p}_T$). The latter allows one to naïvely extend the Standard Model search to the MSSM case: the structure of the Higgs sector predicts at least one scalar in the intermediate mass range, rendering the $\tau\tau$ channel a crucial test of the MSSM [17]. Here, we show how the additional channel $H \to \tau\tau \to e^{\pm}\mu^{\mp}\not{p}_T$ can be isolated, effectively doubling the available statistics for a measurement of the $H\tau\tau$ coupling.

Our analysis is a parton-level Monte Carlo study, using full tree-level matrix elements for the WBF Higgs signal and the various backgrounds. In Section II we describe our calculational tools, the methods employed in the simulation of the various processes, and important parameters. In Section III we demonstrate how forward jet tagging, a b veto, and lepton cuts can be combined to yield an $\approx 2/1$ to $1/2$ signal-to-background (S/B) ratio, depending on the Higgs mass. The different mini-jet patterns in signal and background processes are discussed in Section IV. We describe how they can be used to achieve additional large suppression of the QCD backgrounds relative to the signal. Combined with the results of Section III this yields production cross sections of signal and backgrounds as given in Table IV, which summarizes our results. In Section V we reanalyze the impact on covering the MSSM parameter space and discuss the luminosity requirement at the LHC for which the entire $m_A, \tan\beta$ plane can be covered. A final discussion of our results and conclusions is given in Section VI.

II. CALCULATIONAL TOOLS

We simulate pp collisions at the CERN LHC, $\sqrt{s} = 14$ TeV. All signal and background cross sections are determined in terms of full tree-level matrix elements for the contributing subprocesses and are discussed in more detail below.

For all our numerical results we have chosen $1/\alpha = 128.933$, $M_Z = 91.187$ GeV, and $G_F = 1.16639 \cdot 10^{-5}$ GeV^{-2}, which translates into $M_W = 79.963$ GeV and $\sin^2\theta_W = 0.2310$ when using the tree-level relations between these input parameters. This value for M_W is somewhat lower than the current world average of 80.39 GeV. However, this difference has negligible effects on all cross sections, e.g. the $qq \to qqH$ signal cross section varies by about 0.5% between these two W mass values. The tree level relations between the input parameters are kept in order to guarantee electroweak gauge invariance of all amplitudes. For all QCD effects, the running of the strong coupling constant is evaluated at one-loop order, with $\alpha_s(M_Z) = 0.118$. We employ CTEQ4L parton distribution functions [18] throughout. Unless otherwise noted the factorization scale is chosen as $\mu_f = \min(p_T)$ of the defined jets.

A. The qq → qqH(g) signal process (and background)

The signal can be described, at lowest order, by two single-Feynman-diagram processes, $qq \to qq(WW, ZZ) \to qqH$, i.e. WW and ZZ fusion where the weak bosons are emitted from the incoming quarks [19]. Because of the small Higgs boson width in the mass range of interest, these events can reliably be simulated in the narrow width approximation. From previous studies of $H \to \gamma\gamma$ [20], $H \to \tau\tau$ [16] and $H \to WW$ [6] decays in weak boson fusion we know several features of the signal, which can be exploited here also: the centrally produced Higgs boson tends to yield central decay products (in this case $\tau^+\tau^-$), and the two quarks enter the detector at large rapidity compared to the τ's and with transverse momenta in the 20 to 100 GeV range, thus leading to two observable forward tagging jets.

For the study of a central jet veto, we utilize the results of previous studies where we simulated the emission of at least one extra parton [7,16,21]. This was achieved by calculating the cross sections for the process $qq \to qqHg$, i.e. weak boson fusion with radiation of an additional gluon, and all crossing related processes.

We note that the signal simulations, with decays to tau pairs replaced by decays to W pairs, which in turn decay leptonically, will ultimately also be a source of background for the $H \to \tau\tau$ signal under study.

B. The QCD $t\bar{t}$ + jets backgrounds

Given the H decay signature, the main physics background to our $e^{\pm}\mu^{\mp}\not{p}_T$ signal arises from $t\bar{t} + jets$ production, due to the large top production cross section at the LHC and because the branching ratio $B(t \to Wb)$ is essentially 100%.

The basic process we consider is $pp \to t\bar{t}$, which can be either gg- or $q\bar{q}$-initiated, with the former strongly dominating at the LHC. QCD corrections to this lead to additional real parton emission, i.e. to $t\bar{t} + j$ events. Relevant subprocesses are

$$gq \to t\bar{t}q\,, \quad g\bar{q} \to t\bar{t}\bar{q}\,, \quad q\bar{q} \to t\bar{t}g\,, \quad gg \to t\bar{t}g\,,$$

and the subprocesses for $t\bar{t} + jj$ events can be obtained similarly. For the case of no additional partons, the b's from the decaying top quarks may be identified as the tagging jets. At the same time, we can identify a distinctly different, perturbative region of phase space, where the final-state light quark or gluon gives rise to one tagging jet, and one of the two decay b's is identified as the other tagging jet. Finally, there is a third distinct region of phase space, for the perturbative hard process $pp \to t\bar{t} + jj$, where the final-state light quarks or gluons are the two tagging jets. The $t\bar{t}$ and $t\bar{t}j$ matrix elements were constructed using MADGRAPH [22], while the $t\bar{t}jj$ matrix elements are from Ref. [23].

Decays of the top quarks and W's are included in the matrix elements; however, while the W's are allowed to be off-shell, the top quarks are required to be on-shell. This approximation neglects the contribution from Wt production, which has been shown to be comparable to $t\bar{t}$ rates in studies of the $H \to WW$ signal [8,5]. We will compensate by being conservative in assessing minijet veto probabilities for top backgrounds. Note that these approximations are not critical because backgrounds with real W pairs can be distinguished quite effectively from $\tau\tau$ events and the real top decay backgrounds that we consider will be shown to constitute a minor fraction of the final backgrounds. In the calculation of the $t\bar{t}$ background energy loss from $b \to \ell\nu X$ is included to generate more accurate $\not{p}_T$ distributions. In all cases, the factorization scale is chosen as $\mu_f = \min(E_T)$ of the massless partons/top quarks. As in our earlier work [6], the overall strong coupling constant factors are taken as $(\alpha_s)^n = \prod_{i=1}^{n} \alpha_s(E_{T_i})$, where the product runs over all light quarks, gluons and top quarks.

C. The QCD $b\bar{b}$ + jj background

The semileptonic decays of bottom or charm quarks provide another source of leptons and neutrinos which can be misidentified as tau decays.

These heavy quark pairs are produced strongly and a priori one is dealing with a very large potential background. It can be reduced by several orders of magnitude, however, by requiring the leptons from the decay of the heavy quarks to be isolated. Because of the softer fragmentation function of a c-quark as compared to b-quarks, leptons from charm decay are much less likely to be isolated than b-decay leptons. In the phase space region of interest to us, where both heavy quarks must reside in the central angular region and have substantial transverse momentum, the production cross sections for charm and bottom pairs are roughly equal. As a result we consider only the b-quark background in the following.

In addition to the two high transverse momentum b-quarks, which both must undergo semileptonic decay, two forward tagging jets will be required as part of the signal event selection. The relevant leading order process therefore is the production of $b\bar{b}$ pairs in association with two jets, which includes the subprocesses

$$gg \to b\bar{b}gg\ ,\ \ qg \to b\bar{b}qg\ ,\ \ q_1q_2 \to b\bar{b}q_1q_2\,.$$

The exact matrix elements for the $\mathcal{O}(\alpha_s^4)$ processes are evaluated, including all the crossing related subprocesses, and retaining a finite b-quark mass [23]. The Pauli interference terms between identical quark flavors in the process $q_1q_2 \to b\bar{b}q_1q_2$ are neglected, with little effect in the overall cross section, due to the large difference in the rapidity of the final state light quarks. The factorization and renormalization scales are chosen as in the analogous $t\bar{t}jj$ case.

The semileptonic decay $b \to \nu\ell c$ of both of the b-quarks is simulated by multiplying the $b\bar{b}jj$ cross section by a branching ratio factor of 0.0218 (corresponding to an $e^+\mu^-$ or μ^+e^- final state) and by implementing the $V-A$ decay distributions of the b-quarks in the collinear limit. The collinear approximation for the $b \to \nu\ell c$ decay is appropriate here because the lepton transverse momentum and $\not{p}_T$ cuts to be imposed below force the parent b-quarks to move relativistically in the lab. Denoting the neutrino and charged lepton energy fractions by x_ν and y_ℓ, respectively, the double differential b-quark decay distribution is given by [24]

$$\frac{1}{\Gamma}\frac{d^2\Gamma}{dx_\nu dy_\ell} = \frac{2c}{f(r)}\left(c\,(1-x_\nu)\ [c+(3-c)\,x_\nu\,] + 3ry_\ell\,\frac{(2-c)\,x_\nu + c}{1-x_\nu-y_\ell}\right) \tag{1}$$

assuming an unpolarized initial b-quark. Here $r = m_c^2/m_b^2$, and the dependence on the final state charm quark mass, m_c, is absorbed into the correction term

$$c = \frac{1-r-x_\nu-y_\ell}{1-x_\nu-y_\ell} = 1 - \frac{r}{z_c}\,. \tag{2}$$

Finally, $f(r)$ is the width suppression factor for the $b \to \nu\ell c$ decay due to the finite charm quark mass,

$$f(r) = (1-r^2)(1-8r+r^2) - 12r^2\log r\,. \tag{3}$$

In our numerical simulations we set $m_b = 5.28$ GeV and $m_c = 1.87$ GeV, i.e. we use the lightest meson masses in order to approximately obtain the correct kinematics for the heavy quark decays. In Ref. [25] a factor 100 reduction of the $b\bar{b}$ background was found as a result of lepton isolation for a single $b \to \nu\ell c$ decay, requiring $E_T < 5$ GeV in a cone of radius 0.6 around the charged lepton of $p_{T\ell} > 20$ GeV. In our simulation, after energy smearing of the charm quark jet (see below), we reproduce this reduction factor. The suppression from lepton isolation is smaller for lower $p_{T\ell}$ cuts. We model these effects by using Eq. (1).

Since our suppression of $b \to \nu\ell c$ decays from lepton isolation strongly depends on the energy resolution assumed for the very soft charm quark jet, the determination of heavy quark backgrounds should eventually be repeated with a full detector simulation. We will show, however, that the $b\bar{b}jj$ background is truly negligible after all the selection cuts to be described in this paper. Therefore, the approximate treatment of these backgrounds is sufficient for our purposes.

D. The QCD and EW $\tau^+\tau^- + \mathbf{jj}$ backgrounds

The next obvious backgrounds arise from Z decays to real τ's which then decay leptonically. Thus, we need to study real-emission QCD corrections to the Drell-Yan process $q\bar{q} \to (Z,\gamma) \to \tau^+\tau^-$. For $\tau^+\tau^- jj$ events these background processes include [26]

$$qg \to qg\tau^+\tau^-, \qquad qq' \to qq'\tau^+\tau^-,$$

which are dominated by t-channel gluon exchange, and all crossing-related processes, such as

$$q\bar{q} \to gg\tau^+\tau^-, \qquad gg \to q\bar{q}\tau^+\tau^-.$$

All interference effects between virtual photon and Z-exchange are included. We call these processes collectively the "QCD $\tau\tau jj$" background. Similar to the treatment of the signal processes, we use a parton-level Monte-Carlo program based on the work of Ref. [27] to model the QCD $\tau\tau jj$ background.

From our study of $H \to \tau\tau$ in weak boson fusion [16], we know that the EW (t-channel weak boson exchange) cross section for Zjj production will be comparable to the QCD cross section in the phase space region of interest. We use the results of Ref. [28] for modeling the EW $\tau\tau jj$ background.

The dual leptonic decays of the τ's are simulated by multiplying the $\tau^+\tau^- jj$ cross section by a branching ratio factor of $(0.3518)^2/2$ and by implementing the lepton energy distributions for collinear tau decays, with helicity correlations included as in our previous analysis of $H \to \tau\tau$ [16].

E. The QCD $\mathbf{WW + jj}$ background

We must further consider any other significant source of one electron, one muon and significant $\not{p}_T$ to make a realistic analysis of the backgrounds. An obvious candidate arises from real-emission QCD corrections to W^+W^- production, with subsequent decay of the two W's to electrons or muons. For $W^+W^- jj$ events these background processes include [29]

$$qg \to qgW^+W^-, \qquad qq' \to qq'W^+W^-,$$

which are dominated by t-channel gluon exchange, and all crossing related processes, such as

$$q\bar{q} \to ggW^+W^-, \qquad gg \to q\bar{q}W^+W^-.$$

We call these processes collectively the "QCD $WWjj$" background. To estimate the minijet activity in these events we use the results for QCD $Z + jets$ processes, which are kinematically similar [6,7].

Note that we neglect $W \to \tau\nu \to \ell\nu\nu$ decays in our simulation of $WWjj$ backgrounds. This is justified by the suppressed leptonic branching ratio of the τ decays. We show below that the $WW \to e\mu\nu\nu$ backgrounds are already negligible and, therefore, the extra $W \to \tau\nu$ decays do not need to be analyzed in detail.

F. The EW $\mathbf{WW + jj}$ background

These backgrounds, analogous to QCD $WWjj$ production, arise from W^+W^- bremsstrahlung in quark-(anti)quark scattering via t-channel electroweak boson exchange, with subsequent decay $W^+W^- \to \ell^+\ell^-\not{p}_T$:

$$qq' \to qq'W^+W^-$$

Naïvely, this EW background may be thought of as suppressed compared to the analogous QCD process above. However, it includes electroweak boson fusion, $VV \to W^+W^-$ via s- or t-channel γ/Z-exchange or via VVVV 4-point vertices, which has a momentum and color structure identical to the signal. Thus, it cannot easily be suppressed via cuts.

The matrix elements for these processes were constructed using MADGRAPH [22]. We include charged-current (CC) and neutral-current (NC) processes, but discard s-channel EW boson and t-channel quark exchange processes as their contribution was found to be only $\approx 1\%$, while adding significantly to the CPU time needed for the calculation. In general, for the regions of phase space

containing far-forward and -backward tagging jets, s-channel processes are severely suppressed. We refer collectively to these processes as the "EW $WWjj$" background. Both W's are allowed to be off-shell, and all off-resonance graphs are included. In addition, the Higgs boson graphs must be included to make the calculation well-behaved at large W-pair invariant masses. However, it is convenient to separate continuum W-pair production from the very narrow $H \to W^+W^-$ resonance. We do this by setting M_H to 60 GeV in the EW $WWjj$ background which effectively removes the s-channel Higgs contribution. The $H \to W^+W^-$ background is then calculated separately for ' each Higgs boson mass under consideration. A clean separation of the Higgs boson signal and the EW $WWjj$ background is possible because interference effects between the two are negligible for the Higgs boson mass range of interest.

The effects of additional gluon radiation are estimated by using the results of Refs. [6,7] for EW $\tau\tau jj$ events, which are directly applied here. The EW $\tau\tau jj$ and EW $WWjj$ backgrounds are quite similar kinematically, which justifies the use of the same veto probabilities for central jets.

G. Detector resolution

The QCD processes discussed above lead to steeply falling jet transverse momentum distributions. As a result, finite detector resolution can have a sizable effect on cross sections. These resolution effects are taken into account via Gaussian smearing of the energies of jets/b's and charged leptons. We use

$$\frac{\triangle E}{E} = \frac{3.3}{E} \oplus \frac{0.6}{\sqrt{E}} \oplus 0.03 \,, \tag{4}$$

for central jets (with individual terms added in quadrature), based on ATLAS expectations [5]. For charged leptons we use

$$\frac{\triangle E}{E} = 2\% \,. \tag{5}$$

In addition, finite detector resolution leads to fake missing-transverse-momentum in events with hard jets. An ATLAS analysis [25] showed that these effects are well parameterized by a Gaussian distribution of the components of the fake missing transverse momentum vector, $\vec{\not{p}}_T$, with resolution

$$\sigma(\not{p}_x, \not{p}_y) = 0.46 \cdot \sqrt{\sum E_{T,had}} \,, \tag{6}$$

for each component. In our calculations, these fake missing transverse momentum vectors are added linearly to the neutrino momenta.

III. HIGGS SIGNAL AND BACKGROUNDS

The $qq \to qqH,\ H \to \tau\tau \to e^\pm\mu^\mp\nu\bar{\nu}$ double leptonic decay signal is characterized by two forward jets and the τ decay leptons (e, μ). Before discussing background levels and further details like minijet radiation patterns, we need to identify the search region for these hard Hjj events. The task is identical to the Higgs searches in $qq \to qqH,\ H \to \gamma\gamma, \tau\tau, WW$ which were considered previously [6,7,16,20]. We can thus adopt the strategy of these earlier analyses and start out by discussing a basic level of cuts on the $qq \to qqH,\ H \to \tau\tau$ signal. Throughout this section we assume a Higgs mass of $M_H = 120$ GeV for illustration purposes, but we do not optimize cuts for this mass.

The minimum acceptance requirements ensure that the two jets and two charged leptons are observed inside the detector (within the hadronic and electromagnetic calorimeters, respectively), and are well-separated from each other:

$$\begin{aligned} p_{T_j} \geq 20 \text{ GeV}\,, \quad |\eta_j| \leq 5.0\,, \quad \triangle R_{jj} \geq 0.7\,, \\ p_{T_\ell} \geq 10 \text{ GeV}\,, \quad |\eta_\ell| \leq 2.5\,, \quad \triangle R_{j\ell} \geq 0.7\,. \end{aligned} \tag{7}$$

The charged leptons must be isolated in order to reduce backgrounds from heavy quark decays. Thus a minimum angular distance must be imposed on the electron and the muon signaling the tau decays:

$$\triangle R_{e\mu} \geq 0.4\,. \tag{8}$$

This has negligible effect on the Higgs boson signal.

A feature of the QCD Zjj and $WWjj$ backgrounds is the generally higher rapidity of the Z or W's as compared to the Higgs signal: weak boson bremsstrahlung occurs at small angles with respect to the parent quarks, producing a Z or W's forward of the jets. Thus, we also require both ℓ's to lie between the jets with a separation in pseudorapidity $\triangle\eta_{j,\ell} > 0.7$, and the jets to occupy opposite hemispheres:

$$\begin{aligned} &\eta_{j,min} + 0.7 < \eta_{\ell_{1,2}} < \eta_{j,max} - 0.7\,, \\ &\eta_{j_1} \cdot \eta_{j_2} < 0 \end{aligned} \tag{9}$$

Finally, to reach the starting point for our consideration of the signal and various backgrounds, a wide separation in pseudorapidity is required between the two forward tagging jets,

$$\triangle\eta_{tags} = |\eta_{j_1} - \eta_{j_2}| \geq 4.4\,, \tag{10}$$

leaving a gap of at least 3 units of pseudorapidity in which the charged leptons can be observed. Forward jet tagging has been discussed as an effective technique to separate weak boson scattering from various backgrounds in the past [11–16,6,7,20,21], in particular for heavy Higgs boson searches. Line 1 of Table I shows the effect of the above cuts on the signal and backgrounds for a SM Higgs boson of mass $M_H = 120$ GeV. Overall, about 13% of all $H \to \tau\tau \to e^{\pm}\mu^{\mp}\nu\bar{\nu}$ events generated in weak boson fusion are accepted by the cuts of Eqs. (7)-(10) (for $M_H = 120$ GeV).

As is readily seen from the first line of Table I, the dominant backgrounds are e, μ pairs from heavy quark decays. Of the $t\bar{t}(+jets)$ events 14 fb are from $t\bar{t}$, 360 fb are from $t\bar{t}j$, and the remaining 860 fb arise from $t\bar{t}jj$ production. The additional jets (corresponding to massless partons) are required to be identified as far forward tagging jets. The $t\bar{t}jj$ cross section is largest because the $t\bar{t}$ pair is not forced to have as large an invariant mass as in the first two cases, where one or both b's from the decay of the top quarks must pass the tagging jet cuts.

For the events where only one or none of the b's are identified as a forward jet, the b's will most frequently lie between the two tagging jets, in the region where we search for the W decay leptons. Vetoing events with these additional b jets provides a powerful suppression tool to control the top background [6]. Note that this does *not* require a b-tag, merely rejection of any events that have an additional jet, which in this case would be from a b-quark and its decay products. (It is quite possible that b-tagging could improve this simple rejection criterion, especially in the $p_T < 20$ GeV region.) We discard all events where a b or $\bar{b}$ with $p_T > 20$ GeV is located in the gap region between the tagging jets,

$$p_{T_b} > 20 \text{ GeV}\,, \quad \eta_{j,min} < \eta_b < \eta_{j,max}\,. \tag{11}$$

This leads to a reduction of $t\bar{t}j$ events by a factor 7 while $t\bar{t}jj$ events are suppressed by a factor 100, resulting in cross sections of 50 and 8.7 fb, respectively, at the level of the forward tagging cuts of Eqs. (7)-(10), which are now comparable to the irreducible backgrounds, real taus from Zjj events. (See the second line of Table I.) Note that the much higher b veto probability for $t\bar{t}jj$ events results in a lower cross section than that for $t\bar{t}j$ events, an ordering which will remain even after final cuts have been imposed (see below).

The large $b\bar{b}jj$ background is most effectively reduced by requiring a significant level of missing transverse momentum in the event. The $\not{p}_T$ distributions for the signal and the various backgrounds are shown in Fig. 1. The extremely soft $\not{p}_T$ distribution for $b\bar{b}$ events is mostly due to the stringent lepton isolation requirements. A low transverse momentum of the charm quark in the $b \to c\ell\nu$ decay requires a fairly soft parent b-quark, which in turn does not permit a large $\not{p}_T$ to be carried away by the escaping neutrino. This effect is amplified by the QCD nature of the $b\bar{b}jj$ background which favors the production of low p_T b-quarks in the first place. All other backgrounds involve the decay of one or more massive objects (a Z, Ws, or top quarks) into leptons and neutrinos and thus result in a much harder $\not{p}_T$ distribution. The distributions of Fig. 1 motivate a cut

$$\not{p}_T > 30 \text{ GeV}\,, \tag{12}$$

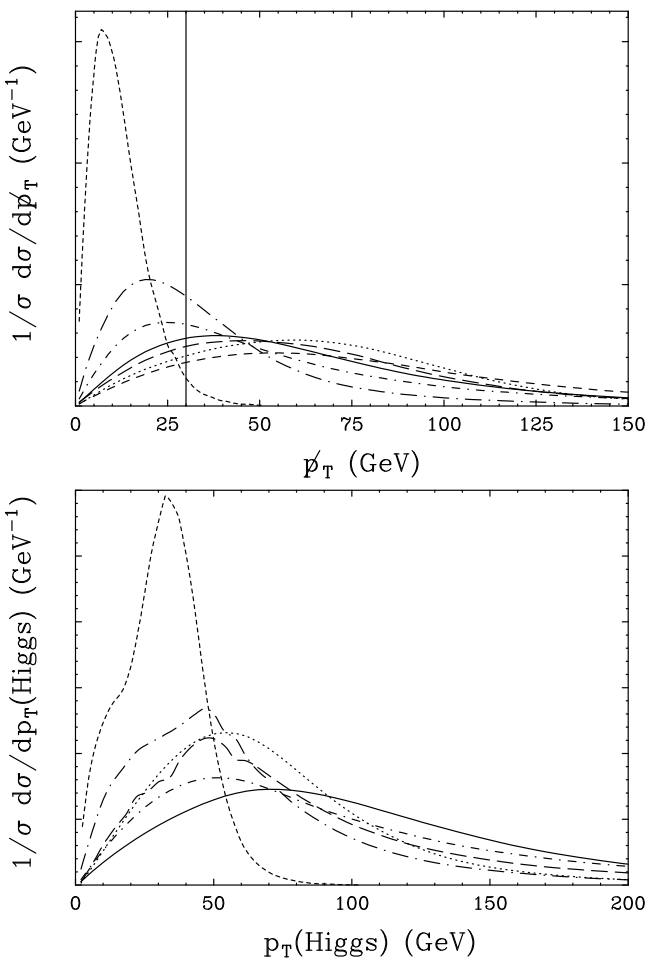

FIG. 1. Upper: Normalized $\not{p}_T$ distribution for the signal (solid) and various backgrounds: $t\bar{t} + jets$ (dotted), $b\bar{b}jj$ (very short dashed), QCD $WWjj$ (long dashed), EW $WWjj$ (short dashed), QCD $\tau\tau jj$ (long dash-dotted) and EW $\tau\tau jj$ (short dash-dotted). The cuts of Eqs. (7)-(11) are imposed. Lower: The same for the normalized p_T distribution of the reconstructed Higgs boson, except that QCD and EW $WWjj$ contributions have been combined (long dashed).

which brings the $b\bar{b}jj$ background to a manageable level. The cross sections after this $\not{p}_T$ cut are shown in the third line of Table I.

A similar reduction of the $b\bar{b}jj$ background can be achieved by a harder lepton transverse momentum requirement than the 10 GeV cut of Eq. (7). However, the signal distribution is quite soft as well and a harder $p_{T\ell}$-cut would lead to an undesirable loss of signal rate. Another option is to make use of

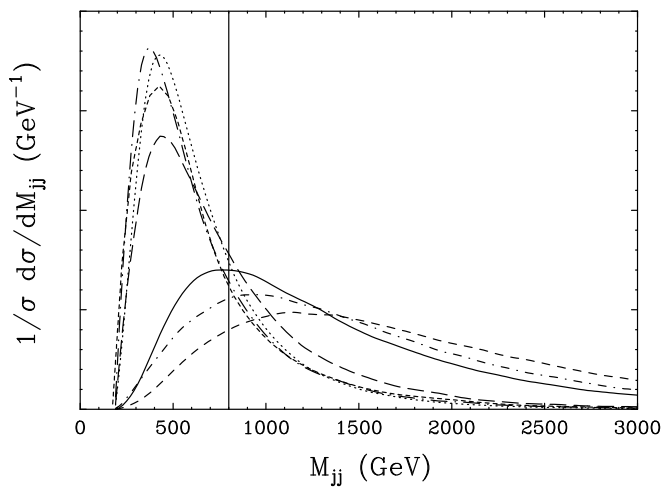

FIG. 2. Normalized invariant mass distribution of the two tagging jets for the signal (solid) and the various backgrounds as in Fig. 1. The cuts of Eqs. (7)-(11) are imposed. (The distributions are essentially unchanged after imposing the additional cut of Eq. 12.)

the transverse momentum of the Higgs boson candidate, defined as the recoil needed to balance the transverse momentum of the observed hadrons in the event. These "Higgs boson" transverse momentum distributions are also plotted in Fig. 1. They are qualitatively similar to $\not{p}_T$ for all processes, but the peak is shifted to lower values than that of the real Higgs boson signal for all backgrounds. While we do not use this distribution here, we point out that it may be useful once a multivariate analysis is performed at the detector level.

QCD processes at hadron colliders typically occur at smaller invariant masses than EW processes, due to the dominance of gluons at small Feynman x in the incoming protons. We observe this behavior here, as shown in Fig. 2. The three $t\bar{t} + jets$ backgrounds have been combined for clarity, even though their individual distributions are slightly different. One can significantly reduce the QCD backgrounds by imposing a lower bound on the invariant mass of the two tagging jets:

$$M_{jj} > 800 \text{ GeV} . \tag{13}$$

Resulting cross sections are shown in the fourth line of Table I.

For significant further reduction of the various backgrounds, reconstruction of the tau-pair invariant mass [30] is necessary. Due to the large mass of the decaying Higgs boson and also because of its large transverse momentum (see Fig. 1) the produced taus are moving relativistically in the laboratory frame. As a result the tau direction closely follows the direction of the corresponding observed decay lepton. Since the transverse momentum of the Higgs boson is known (it is given by the vectorial sum of charged lepton p_T's and missing transverse momentum) the momentum parallelogram in the transverse plane allows one to extract the fractions of the two tau momenta which are carried by the two charged leptons. We denote these momentum fractions by x_{τ_1}, x_{τ_2} in the following. This reconstruction works only if the taus are not emitted back-to-back in the transverse plane and we therefore impose the technical cut

$$\cos\phi_{e\mu} \; > \; -0.9 \, . \qquad (14)$$

The resulting x_{τ_1}, x_{τ_2} distributions are shown in the form of a scatter plot of unweighted events in Fig. 3. The distribution for real tau pairs is shown only for the Higgs boson signal because the plot for $\gamma^*/Z \to \tau\tau$ looks virtually identical.

For real τ decays, the $\not{p}_T$ vector must lie between the two leptons, and apart from finite detector resolution the reconstruction must yield $0 < x_{\tau_{1,2}} < 1$. For the WW and $t\bar{t}$ backgrounds, however, the collinear approximation is not valid because the W's and top quarks receive only modest boosts in the lab. In this case, the $\not{p}_T$ vector will rarely lie between the two leptons, and an attempt to reconstruct a τ pair will result in $x_{\tau_1} < 0$ or $x_{\tau_2} < 0$ for a significant fraction of the events [6]. Many others end up in the unphysical region $x_\tau > 1$. The scatter plot of Fig. 3 suggests the real τ-reconstruction cuts

$$x_{\tau_1},\, x_{\tau_2} > 0 \, , \quad x_{\tau_1}^2 + x_{\tau_2}^2 < 1 \, . \qquad (15)$$

Once the momentum fractions carried by the e, μ-pair are known, the invariant mass of the tau-pair is given by

$$M_{\tau\tau} = m_{e\mu}/\sqrt{x_{\tau_1} x_{\tau_2}} \, . \qquad (16)$$

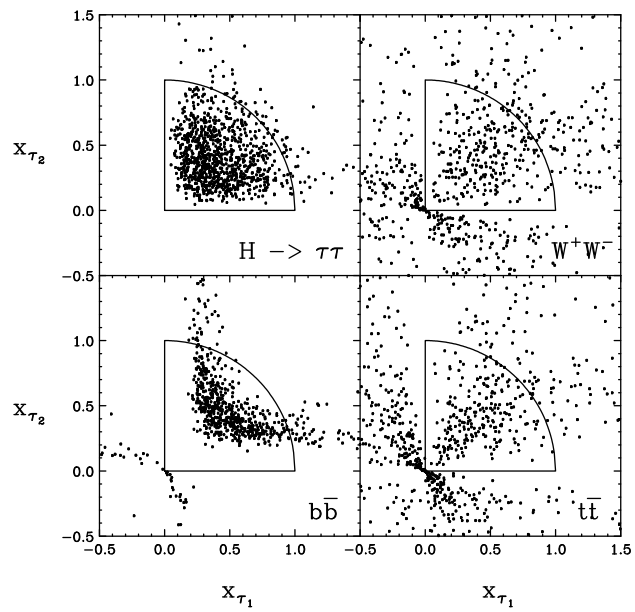

FIG. 3. Scatter plots of x_{τ_1} v. x_{τ_2} with the cuts of Eqs.(7)-(14), for the 120 GeV Hjj signal, $b\bar{b}jj$, $WWjj$ and $t\bar{t} + jets$ reducible backgrounds. The number of points in each plot is arbitrary and corresponds to significantly higher integrated luminosities than expected for the LHC. The solid lines indicate the cuts of Eq. (15).

The reconstructed tau-pair invariant mass distributions for the combined W^+W^- and $t\bar{t}$ backgrounds, for $b\bar{b}jj$ events and for the QCD and EW Zjj events are shown in Fig. 4, after the back-to-back cut of Eq. (14). The $b\bar{b}jj$ background is almost completely concentrated in the small $M_{\tau\tau}$ region and $\gamma^*/Z + jj$ events are strongly peaked at $M_{\tau\tau} = M_Z$. When searching for a Higgs boson mass peak well above M_Z, both backgrounds are drastically reduced. As is indicated by the width of the Z peak in Fig. 4, a resolution of about 10% is possible for the reconstructed tau-pair invariant mass, which agrees well with earlier results obtained with full detector simulations for $A \to \tau\tau$ by ATLAS [25]. Here we are interested in SM Higgs bosons with a mass in the range 100 GeV $< M_H <$ 150 GeV. As a result we need to consider only backgrounds which lead to a reconstructed $M_{\tau\tau}$ in the range

$$90 \text{ GeV} \; < M_{\tau\tau} < \; 160 \text{ GeV} \, . \qquad (17)$$

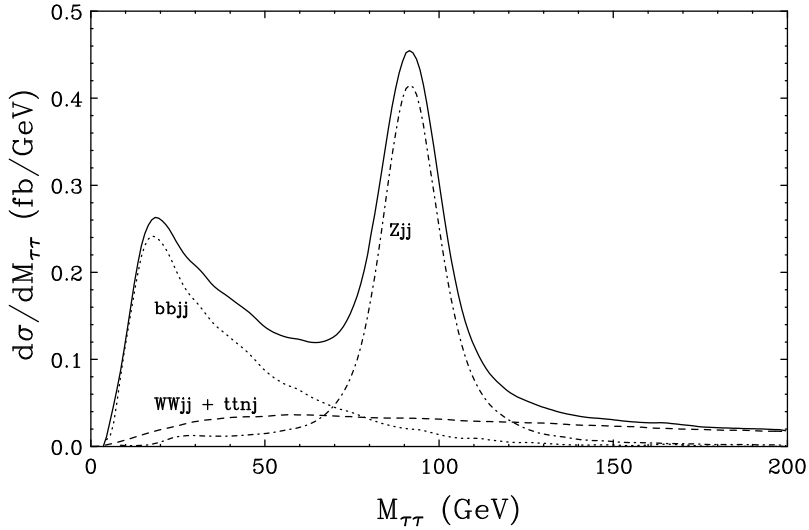

FIG. 4. Reconstructed tau-pair mass distribution for $WWjj$ and $t\bar{t}+jets$ events (dashed line), $b\bar{b}jj$ events (dotted line) and QCD+EW Zjj events (dash-dotted line). The combined curves are also shown (solid). The cuts of Eqs. (7)-(14) are imposed.

The reduced background level due to this tau-pair mass cut is shown in the last line of Table I.

Clearly, Higgs mass reconstruction is a very powerful background suppression tool, in particular for $b\bar{b}jj$ events which mostly populate the low $M_{\tau\tau}$ region. This means that the background cross sections in Table I exaggerate the background level and one should rather consider the expected rates in the vicinity of the Higgs boson mass peak. Given the expected mass resolution, we only need to consider background events within ± 10 GeV of the peak. In Table II we have summarized these cross sections at the various cut levels for the example of a Higgs boson at $M_H = 120$ GeV. Within the cuts of Eqs. (7)-(15) we have achieved a signal to background (S/B) ratio of 1/1.

Yet another significant difference between signal and some backgrounds is the angular distribution of the charged decay leptons, $e^{\pm}$ and $\mu^{\mp}$, relative to each other. In the case of the Higgs signal, the high p_T of the Higgs boson results in a tau pair, and therefore charged decay leptons, which are emitted fairly close together in the lab frame. In the case of the heavy quark backgrounds, this correlation is not reproduced, in particular when viewed as lepton separation in the lego plot (see Fig. 5). For the $b\bar{b}jj$ background, for example, a large rapidity separation is induced by the conflicting requirements of a large tau-pair invariant mass and the low lepton transverse momenta surviving the lepton isolation cuts. The lepton correlations can be exploited by imposing a lepton pair angular cut:

$$\triangle R_{e\mu} < 2.6\,. \tag{18}$$

This cut acts primarily against the $t\bar{t}+jets$ and $b\bar{b}jj$ backgrounds, which are already at a quite low level. We select the value 2.6 conservatively to retain more signal rate, in particular for large Higgs boson masses, close to $M_H = 150$ GeV.

At this level of cuts we consider one final background, an additional source of $e+\mu+\not{p}_T$ from Higgs production itself, via $H \to WW$ decay. Real or slightly virtual W's are produced as opposed to real τ's, so the search for real τ's outlined above will restrict the contribution from this decay channel. However, most of the other cuts we have described isolate Higgs production only, and even the lepton angular cut will select $H \to WW$ events due to the strong anti-correlation of the W spins, which leads to the e, μ pair being emitted preferentially together in the rest frame of the Higgs boson [8];

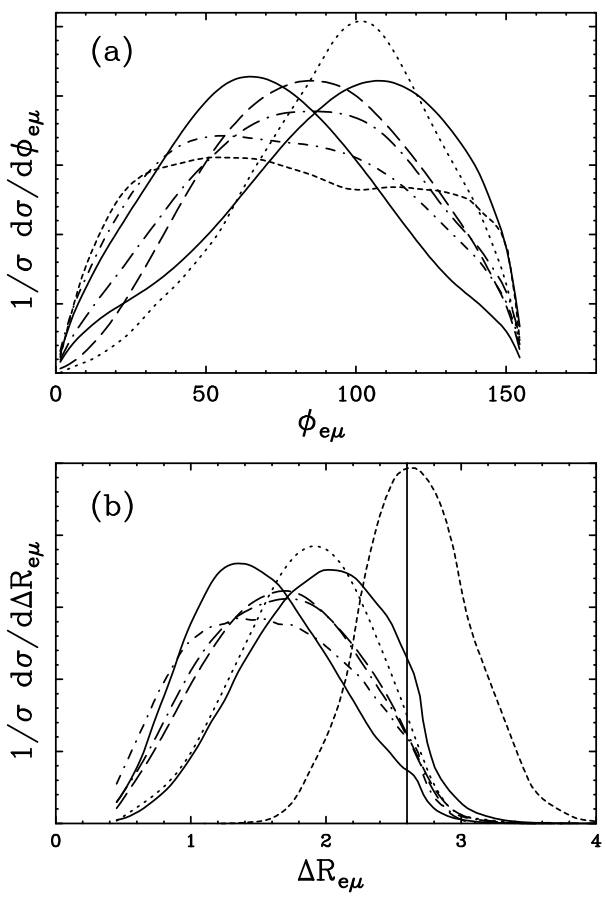

FIG. 5. Normalized angular distributions of the charged leptons: a) azimuthal opening angle and b) separation in the lego plot. Results are shown for Higgs boson masses of 100 and 150 GeV (solid lines) and for the various backgrounds: $t\bar{t} + jets$ (dotted), $b\bar{b}jj$ (very short dashed), combined QCD and EW $WWjj$ (long dashed), QCD $\tau\tau jj$ (long dash-dotted) and EW $\tau\tau jj$ (short dash-dotted). The cuts of Eqs. (7)-(15),(17) are imposed.

the large transverse boost of the Higgs boson in the lab only enhances this angular correlation [6]. The large WW branching ratio compared to that for $\tau\tau$ over the upper end of the mass range which we are considering ($\approx 130 - 150$ GeV), then leads to a background component which cannot be neglected. Table III demonstrates this via a comparison of the $H \to \tau\tau$ signal and $H \to WW$ background over the mass range of interest, after all cuts previously discussed have been imposed.

Another distribution of interest is the lepton-pair invariant mass, $m_{e\mu}$, which is shown in Fig. 6

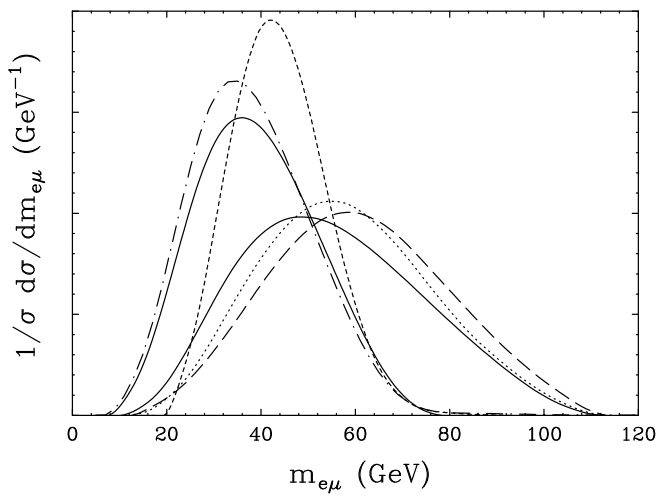

FIG. 6. Normalized dilepton invariant mass distribution, after the cuts of Eqs. (7)-(15), (17),(18) have been imposed. Results are shown for Higgs boson masses of 100 and 150 GeV (solid lines) and for the various backgrounds as in Fig. 1, except that the QCD and EW $\tau\tau jj$ backgrounds have been combined for clarity (dash-dotted line), and the long-dashed line corresponds to the combined QCD + EW $WWjj$ background.

for Higgs masses of $M_H = 100$ GeV and 150 GeV and for the various backgrounds. As is readily seen, the $t\bar{t} + jets$ and $WWjj$ backgrounds prefer high values of $m_{e\mu}$, while the real-tau backgrounds cluster at low invariant mass. A cut on this observable would have to be Higgs mass specific. We therefore do not cut on $m_{e\mu}$, but instead mention it as an additional distinguishing characteristic of the Higgs signal at a very advanced level of cuts.

While we do not impose any further cuts at this point, we should include an estimate of the total rate loss due to various detector efficiencies, to make closer contact with experimental expectations. Based on discussions with ATLAS and CMS experimentalists, we apply an additional factor 0.86^2 for the ID efficiency of the two tagging jets, and a factor 0.95^2 for the ID efficiency of the two charged leptons, e and μ. The combined detection efficiencies are reflected in line 7 of Table II. We note that the high efficiency for lepton triggering and identification may not hold for all leptons down to $p_T = 10$ GeV, but we do not expect losses

TABLE I. Signal rates $\sigma \cdot B(H \to \tau\tau \to e^{\pm}\mu^{\mp}\not{p}_T)$ for $M_H = 120$ GeV and corresponding background cross sections, in pp collisions at $\sqrt{s} = 14$ TeV. Results are given for various levels of cuts and are labeled by equation numbers discussed in the text. No constraint on the reconstructed $\tau\tau$ invariant mass is imposed, except in the last line which requires 90 GeV< $m_{\tau\tau}$ <160 GeV. All rates are given in fb.

cuts	Hjj	QCD $\tau\tau jj$	EW $\tau\tau jj$	$t\bar{t} + jets$	$b\bar{b}jj$	QCD $WWjj$	EW $WWjj$	S/B
forward tags (7)-(10)	2.2	57	2.3	1230	1050	4.9	3.3	1/1100
+ b veto (11)				72				1/550
+ $\not{p}_T$ (12)	1.73	29	1.57	62	29	4.1	2.9	1/74
+ M_{jj} (13)	1.34	10.3	1.35	16.3	10.4	1.60	2.6	1/32
+ non-τ reject. (14,15)	1.15	5.2	0.63	0.31	0.42	0.032	0.042	1/5.8

TABLE II. Signal rates $\sigma \cdot B(H \to \tau\tau \to e^{\pm}\mu^{\mp}\not{p}_T)$ for a SM Higgs boson of $M_H = 120$ GeV and corresponding background cross sections, within ± 10 GeV mass bins. Results are given for various levels of cuts and are labeled by equation numbers discussed in the text. On line seven we include an overall efficiency factor for identification of tagging jets and leptons, as discussed in the text. On line eight the minijet veto is included, with $p_T^{veto} = 20$ GeV. All rates are given in fb.

cuts	$H \to \tau\tau$ signal	$H \to WW$ bkgd	QCD $\tau\tau jj$	EW $\tau\tau jj$	$t\bar{t} + jets$	$b\bar{b}jj$	QCD $WWjj$	EW $WWjj$	S/B
forward tags (7-10)	1.34		4.7	0.18	45	8.2	0.18	0.11	1/44
+ b veto (11)					2.6				1/12
+ $\not{p}_T$ (12)	1.17		2.3	0.12	2.0	0.28	0.12	0.08	1/4.1
+ M_{jj} (13)	0.92		0.67	0.10	0.53	0.13	0.049	0.073	1/1.7
+ non-τ reject. (14,15)	0.87		0.58	0.10	0.09	0.10	0.009	0.012	1/1
+ $\triangle R_{e\mu}$ (18)	0.84	0.023	0.52	0.086	0.087	0.028	0.009	0.011	1.1/1
+ ID effic. ($\times 0.67$)	0.56	0.015	0.34	0.058	0.058	0.019	0.006	0.008	1.1/1
$P_{surv,20}$	$\times 0.89$	$\times 0.89$	$\times 0.29$	$\times 0.75$	$\times 0.29$	$\times 0.29$	$\times 0.29$	$\times 0.75$	-
+ minijet veto (19)	0.50	0.014	0.100	0.043	0.017	0.006	0.002	0.006	2.7/1

TABLE III. Cross section times branching ratio for the $H \to \tau\tau$ signal vs. $H \to WW$ background, for the mass range of interest. The cuts of Eqs. (7)-(15),(18) are imposed, and rates correspond to $m_{\tau\tau} = M_H \pm 10$ GeV mass bins around the Higgs boson mass.

M_H	100	105	110	115	120	125	130	135	140	145	150
B($H \to \tau\tau$)$\cdot\sigma$ (fb)	1.04	1.03	0.98	0.93	0.84	0.74	0.62	0.51	0.39	0.27	0.19
B($H \to WW$)$\cdot\sigma$ (fb)	0.002	0.005	0.00	0.015	0.024	0.034	0.045	0.057	0.067	0.072	0.076

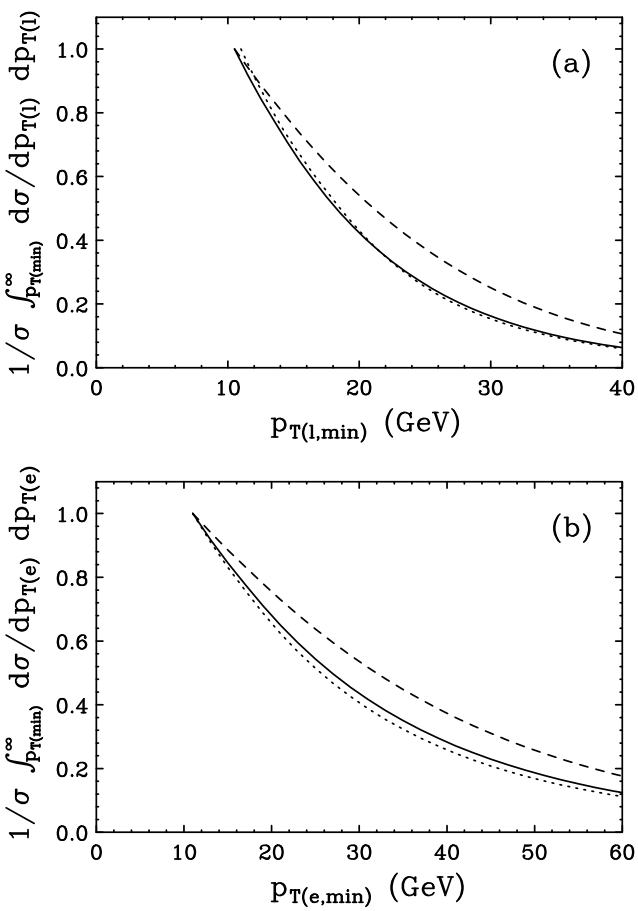

FIG. 7. Integrated charged lepton p_T distributions after the cuts of Eqs. (7)-(15),(17),(18) have been imposed. Shown are events fractions above a minimal lepton p_T as compared to a threshold of 10 GeV for (a) the minimal e or μ transverse momentum, $p_{T\ell,min}$, and (b) the electron transverse momentum, $p_{T,e}$. Results are shown for Higgs boson masses of $M_H = 100$ GeV (solid) and 150 GeV (dashed line) and for the combined background (dotted).

to be large enough to render our estimate grossly optimistic.

The consequences of higher effective lepton transverse momentum thresholds are explored in Fig. 7. An increase of both the electron and the muon threshold to e.g. $p_{T,\ell} > 15$ GeV would lead to a signal loss of order 30%, with a slight improvement of S/B, as can be read off Fig. 7(a). An increase of only the electron threshold to this value would reduce the $H \to \tau\tau$ signal by less than 20% (see Fig. 7(b)). p_T thresholds may be as high as 20 GeV for electrons but can be as low as 6 GeV for triggering on muons [5,31]. Given the complex nature of the signal at hand, containing electrons, muons, missing transverse momentum and jets, the issue of devising an effective trigger, at low and high luminosity, needs to be addressed within a full detector study and cannot be performed by us. We want to emphasize the premium for low lepton p_T thresholds, however.

IV. RADIATION PATTERNS OF MINIJETS

If we are to veto central b jets to reduce the $t\bar{t} + jets$ background to a manageable level, we must take care to correctly estimate higher-order additional central partonic emission in the signal and backgrounds [6]. Fortunately, due to the absence of color exchange between the two scattering quarks in EW processes, which includes our Hjj signal, we expect soft gluon emission mainly in the very forward and very backward directions. For QCD processes, on the other hand, which are dominated by t-channel color octet exchange, soft gluon radiation occurs mainly in the central detector. Thus, when considering additional central radiation with $p_T \geq 20$ GeV to match our b veto condition, we will reject QCD backgrounds with much higher probability than the EW processes. Our b veto is then automatically also a minijet veto, a tool for QCD background suppression which has been previously studied in great detail for Hjj production at hadron colliders [15,7,16,32].

Largely following the analysis of Ref. [21] for the analogous EW Zjj process which would be used to "calibrate" the tool at the LHC, we veto additional central jets in the region

$$p_{Tj}^{\rm veto} > p_{T,\rm veto}\,, \tag{19a}$$

$$\eta_{j,min}^{\rm tag} < \eta_j^{\rm veto} < \eta_{j,max}^{\rm tag}\,, \tag{19b}$$

where $p_{T,\rm veto}$ may be chosen based on detector capabilities and expected minijet production from double parton scattering. Here we take $p_{T,\rm veto} = 20$ GeV.

The determination of veto efficiencies for the QCD backgrounds encounters the problem that we are interested in the phase space region where additional soft parton emission is very likely. In a fixed order perturbative calculation of cross sections with an additional soft central jet of $p_{Tj} > p_{T,\mathrm{veto}}$ this leads to a "3-jet" cross section (counting the two forward tagging jets plus the soft central veto-jet) which often exceeds the corresponding hard "2-jet" cross section considered in the previous Section. The occurrence of $\sigma_{3\,jet} > \sigma_{2\,jet}$ indicates that effects of multiple soft gluon emission must be taken into account. We have analyzed this problem in detail before [16,21,6,7] and found that two very different procedures give consistent results for the veto probabilities. The first, the truncated shower approximation (TSA) [33], regularizes the soft parton p_T distribution so as to reproduce the p_T distribution of the hard recoil system which is expected from a full resummation calculation, while preserving the normalization of the hard 2-jet cross section. The second, the "exponentiation model" assumes that soft gluon radiation approximately exponentiates. This implies that central veto jet multiplicities effectively follow a Poisson distribution with mean $\bar{n}_{jet} = \sigma_3/\sigma_2$ [34]. Both methods use perturbative cross sections for 2- and 3-jet cross sections. The advantage is that QCD matrix elements at tree level contain the full information on angular distributions and hardness of additional jet emission. A parton shower approach would not immediately give reliable answers unless both color coherence and the choice of scale are implemented correctly, matching the answer given by QCD matrix elements for sufficiently hard partons.

In the following we directly use the results of Ref. [6,7], which considered Higgs production by WBF and background processes in phase space regions for the jets that are virtually identical to the ones considered here. In contrast to our early studies [16,21], the veto candidates are defined jets ($p_T > 20$ GeV) anywhere between the tagging jets, i.e. they are searched for in a somewhat larger rapidity region than the τ decay leptons (see Eq. (9)), which have to be at least 0.7 units of rapidity away from the tagging jets. The choice of Eq. (19b) allows for more suppression of the backgrounds than the more restrictive selection.

The resulting veto survival probabilities are summarized in line eight of Table II. These values were determined with 3-jet Monte Carlo simulations for the Higgs signal and QCD and EW Zjj production [6,7]. The results for QCD Zjj production are also used for QCD $WWjj$ production, due to the similarity of the subprocesses, and are taken as well for the $t\bar{t}+jets$ and $b\bar{b}jj$ backgrounds. We have separately examined the expected survival probabilities for $t\bar{t} + jets$ for the exponentiation model in Refs. [6,7], finding somewhat higher veto probabilities than for Zjj events. Because of the uncertainties in the determination of veto probabilities we prefer the more conservative estimates here. Note, however, that even without considering any additional minijets, the $t\bar{t}$ backgrounds are very small (see line seven of Table II), mitigating any concern over minijet veto probabilities. While the veto survival probabilities of Table II are estimates only, they can be independently determined at the LHC in processes like Zjj and Wjj production [21,28].

So far we have considered a single Higgs boson mass of 120 GeV only. We must extend our results to a larger range of M_H. The expected number of signal and background events for 100 GeV $\leq M_H \leq$ 150 GeV and an integrated luminosity of 60 fb^{-1} are shown in Table IV. In the fourth line of Table IV we show the S/B rate, and in the fifth line we show the Poisson probability for the combined backgrounds to fluctuate up to the signal level, in terms of the equivalent Gaussian significances which can be expected in the experiment on average. Low luminosity running is assumed, i.e. no efficiency losses due to overlapping minimum bias events are considered.

V. IMPLICATIONS FOR THE MSSM

The $H \to \tau\tau$ decay mode has proven especially useful in case of the minimal supersymmetric extension of the Standard Model [17]. In the MSSM

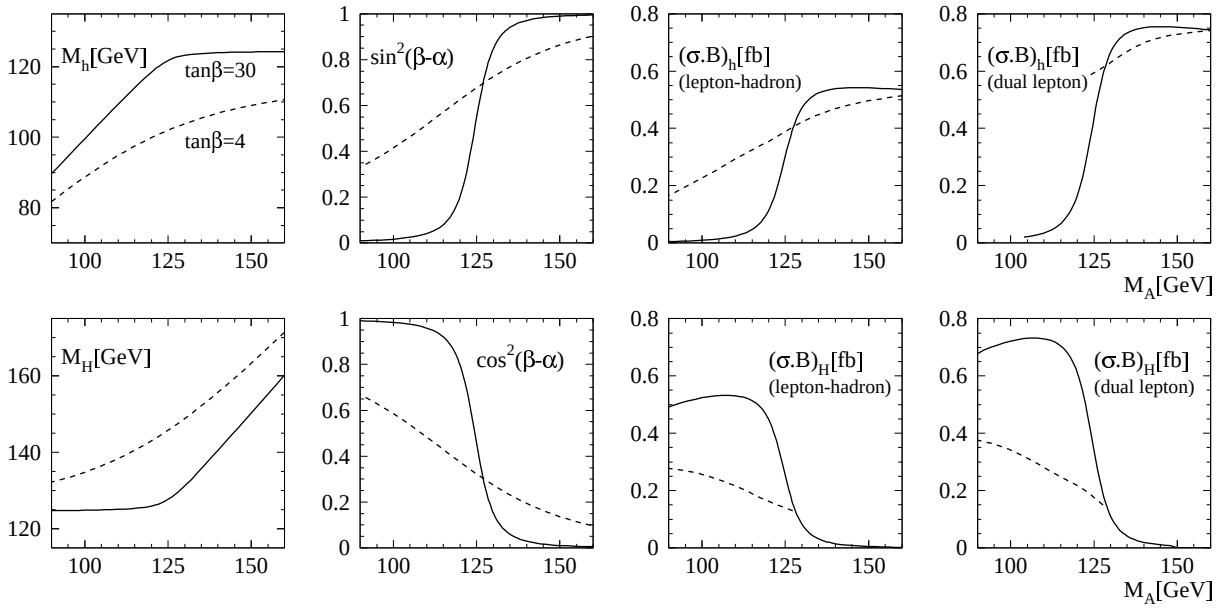

FIG. 8. Variation of Higgs boson masses, couplings to gauge bosons, and signal rates for the two $\tau\tau$ channels as a function of the pseudoscalar Higgs boson mass. The complementarity of the two scalar plateau states is shown for $\tan\beta = 4, 30$. Other MSSM parameters are set to $\mu = 200$ GeV, $M_{\rm SUSY} = 1$ TeV, and maximal mixing.

the neutral CP even Higgs boson states form two mass eigenstates, the properties of which are usually described as functions of $\tan\beta$ and the pseudoscalar mass M_A. For very large or very small values of M_A the scalar masses M_h or M_H approach a plateau, as shown in Fig. 8. These plateau states have masses below $\lesssim 130$ GeV [9,10], dependent on the value of $\tan\beta$. Together with the projected limits from the Zh and ZH search at LEP2 this yields exactly the mass window where the WBF $H \to \tau\tau$ mode is most promising, as shown in Table IV.

The couplings of the MSSM Higgs bosons to W, Z and τ pairs are given by the SM coupling and a multiplicative SUSY factor which for the weak bosons are

$$\begin{aligned} \eta_{VVh} &= \sin(\beta-\alpha)\,, \\ \eta_{VVH} &= \cos(\beta-\alpha)\,, \end{aligned} \tag{20}$$

while for down-type fermions the factors are

$$\begin{aligned} \eta_{\tau\tau h} &= -\frac{\sin\alpha}{\cos\beta} \\ &= \sin(\beta-\alpha) - \tan\beta\,\cos(\beta-\alpha)\,, \\ \eta_{\tau\tau H} &= \frac{\cos\alpha}{\cos\beta} \\ &= \cos(\beta-\alpha) + \tan\beta\,\sin(\beta-\alpha)\,, \end{aligned} \tag{21}$$

where α is the mixing angle between the two CP even Higgs boson states. On the M_h and M_H plateaus one finds $\alpha \approx \beta - \pi/2$ and $\alpha \approx -\beta$, leading to $\eta_{VVh} \approx 1$ on the M_h plateau and $\eta_{VVH} \approx 1$ on the M_H plateau (see Fig. 8). The $\tau\tau$ SUSY factors on the plateaus are dominated by the first terms in Eq. (21), again rendering unity.[1] Thus, in both

[1]The case of vanishing $\eta_{\tau\tau h}$ or $\eta_{\tau\tau H}$ has previously been discussed in detail [17]: $h, H \to \gamma\gamma$ would be dramatically enhanced and become the dominant discovery mode.

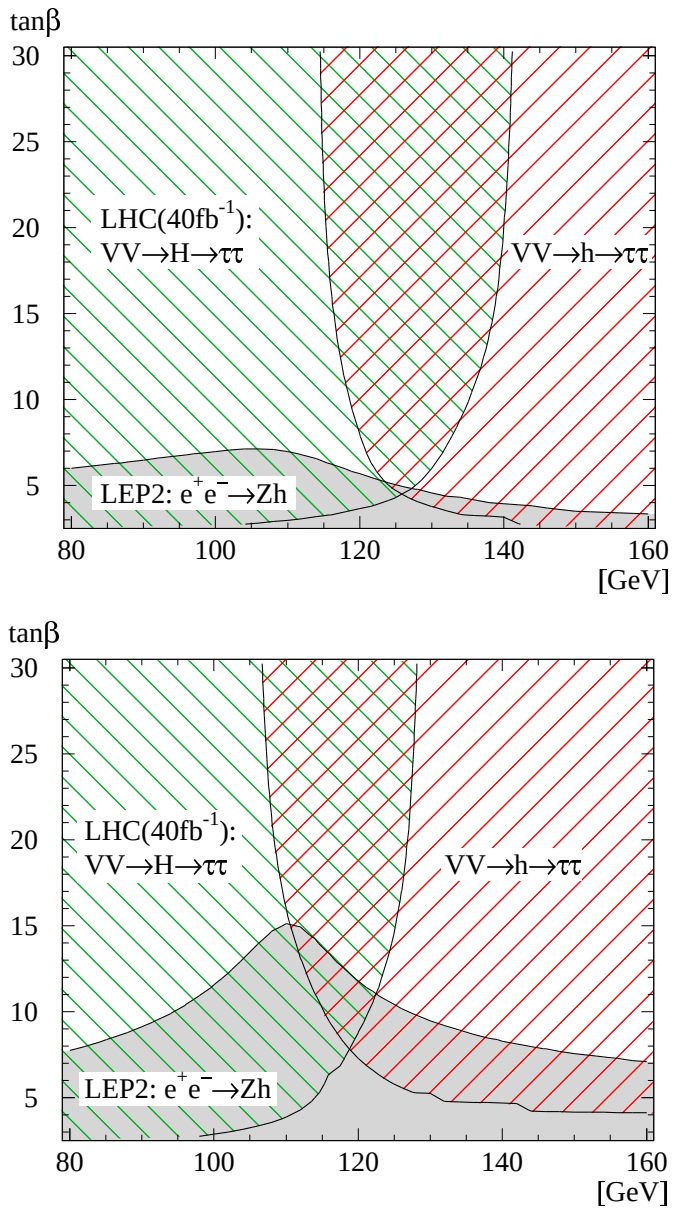

FIG. 9. 5σ discovery contours for $h, H \to \tau\tau$ at the LHC with $\lesssim 40$ fb^{-1}. They are complemented by the current LEP2 limits. The SUSY parameters are set to $\mu = 200$ GeV, $M_{\rm SUSY} = 1$ TeV, and maximal mixing (upper) and no mixing (lower).

plateau regions the situation is very similar to the SM case discussed above. As illustrated in Fig. 8 these plateau states are numerically approached for moderate M_A values already, as long as $\tan\beta$ does not become too small, which would be in conflict with LEP2 limits. In fact, the MSSM branching ratio $B(h, H \to \tau\tau)$ is even slightly enhanced compared to the SM case [35].

Previously we have analyzed the semileptonic $\tau\tau$ decay mode $h/H \to \tau\tau \to e/\mu^\pm h^\mp \not{p}_T$ [17]. To the semileptonic channel we can now add the signal expected in the purely leptonic mode, $h/H \to \tau\tau \to e^\pm\mu^\mp\not{p}_T$. In this extended analysis we change our definition of the "MSSM Higgs boson signal" as compared to the previous analysis, which yielded a 5σ coverage of the entire parameter space with ≈ 100 fb^{-1} luminosity. In the WBF $\tau\tau$ mode the SM and the MSSM analyses are exactly the same, namely scanning the invariant $\tau\tau$ mass distribution for a Higgs mass peak and finding the probability that the excess events could arise from a fluctuation of the background within a ± 10 GeV mass window. For values of M_A in the transition region the reconstructed mass peaks from $h \to \tau\tau$ and $H \to \tau\tau$ decays will be close to each other. Hence, the tail of the invariant mass distribution resulting from the non-plateau state will add to the plateau state signal, reducing the required luminosity for a complete coverage to ≈ 80 fb^{-1} for the semileptonic channel alone.

For each of the two discovery modes j (semileptonic and purely leptonic) we calculate the probability P_j for the background to fluctuate and produce all expected signal+background events. P_1 and P_2 are combined to $P_1P_2(1 - \log(P_1P_2))$ [36]. This probability instead of the naïve product of the two single channel probabilities is then translated into the luminosity required for a 5σ discovery.[2] However, since we consider two channels of similar strength we do not observe significant influence of the statistical treatment on the final numbers.

To estimate the required luminosity for complete coverage of the MSSM parameter space with an expected 5σ signal we chose the supersymmetric mass scale $M_{\rm SUSY}$ as 1 TeV and vary the trilinear stop coupling A_t between 0 (no mixing) and $\sqrt{6}\, M_{\rm SUSY}$ (maximal mixing). The latter yields the

[2]Some analyses prefer to chose the Bayesian instead of the Frequentist approach, which would lead to a slight decrease in our required luminosity.

TABLE IV. Number of expected events for a SM Hjj signal in the $H \to \tau\tau \to e^{\pm}\mu^{\mp}\not{p}_T$ channel, for a range of Higgs boson masses. Results are given for 60 fb^{-1} of data at low luminosity running, and application of all efficiency factors and cuts, including a minijet veto. As a measure of the Poisson probability of the background to fluctuate up to the signal level, the last line gives σ_{Gauss}, the number of Gaussian equivalent standard deviations.

M_H	100	105	110	115	120	125	130	135	140	145	150
$\epsilon \cdot \sigma_{sig}$ (fb)	0.62	0.61	0.58	0.55	0.50	0.44	0.37	0.30	0.23	0.16	0.11
N_S	37.4	36.5	35.0	32.8	30.0	26.3	22.3	18.0	13.7	9.9	6.5
N_B	67.7	45.4	27.4	16.8	11.2	8.4	7.1	6.4	6.1	5.9	5.7
S/B	0.6	0.8	1.3	2.0	2.7	3.2	3.1	2.8	2.2	1.7	1.1
σ_{Gauss}	4.1	4.8	5.6	6.4	6.8	6.7	6.1	5.3	4.3	3.2	2.2

maximal plateau mass. However, from Table IV we conclude that our limit is very robust against effects which move the plateau masses. As a complementary measurement small values of $\tan\beta$ are excluded through the Zh, ZH limits from LEP2. This assures that the Higgs mass peak is sufficiently separated from the Z background peak. We are aware that other LEP2 channels like Ah, AH or the Tevatron RunII search will probe a fraction of the MSSM parameter space, but we do not need to rely on them for complete coverage of the MSSM parameter space. The results are shown in Fig. 9: combining the two tau decay channels leads to a required luminosity of $\lesssim 40$ fb^{-1} for a 5σ observation, with a comfortable overlap in the no-mixing scenario. This number still depends on the LEP2 reach, which we conservatively fix to the current limits [37]. The transition region of moderate pseudoscalar masses (which limits the reach) exhibits one additional feature: if the luminosity is large enough there will be a growing region where both the light and the heavy scalar will appear as peaks in the invariant mass spectrum. This would lead to a unique opportunity to measure the mixing angles in the MSSM Higgs sector.

VI. DISCUSSION

The results summarized in Table IV show that it is possible to isolate a low-background $qq \to qqH$, $H \to \tau\tau \to e^{\pm}\mu^{\mp}\not{p}_T$ signal for the SM Higgs boson at the LHC. Counting rates will be sufficiently large to obtain a better than 5σ signal with ≈ 60 fb^{-1} of data for the mass range 105-135 GeV. Extending the observability region down to 100 GeV still requires less than 90 fb^{-1} of data, assuming low luminosity conditions. Above $M_H = 140$ GeV the signal quickly deteriorates, due to the falling branching ratio for the $H \to \tau\tau$ mode. These results are comparable to those for the $H \to \tau\tau \to h^{\pm}\ell^{\mp}\not{p}_T$ channel [7,16], except as M_H approaches 145-150 GeV. In this high mass range the purely leptonic $\tau\tau$ decay signal receives substantial backgrounds from $H \to WW$. Combined with the semileptonic channel discussed in Refs. [7,16] one effectively doubles the available statistics for the $H \to \tau\tau$ decay mode, making observation of this decay possible with significantly less than 60 fb^{-1} of data, and ultimately providing a number of cross checks for the individual analyses. In the MSSM framework the combination of the two decay modes yields a 5σ signal for $\lesssim 40$ fb^{-1} of data with an arbitrary choice of MSSM parameters which are still allowed by LEP data.

The expected purity of the signal is demonstrated in Fig. 10, where the reconstructed $\tau\tau$ invariant mass distribution for a SM Higgs boson of mass 120 GeV is shown, together with the various backgrounds, after application of all cuts, ID efficiencies and a minijet veto. This purity is made possible because the weak boson fusion process, together with the $H \to \tau\tau \to e^{\pm}\mu^{\mp}\not{p}_T$ decay, provides

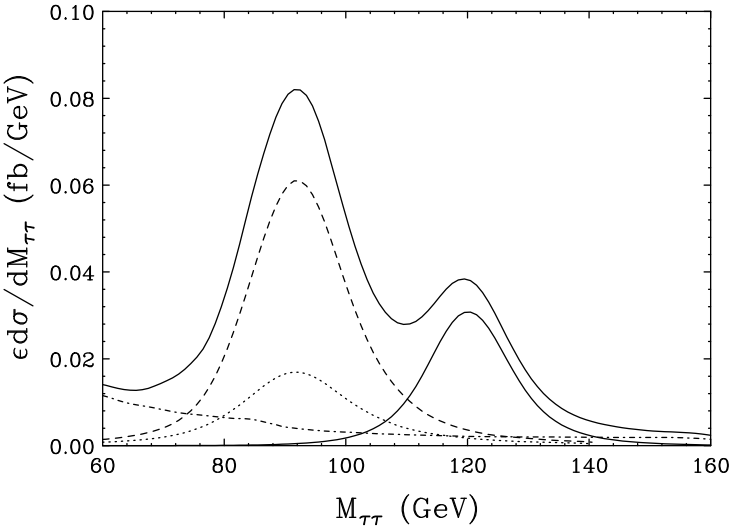

FIG. 10. Reconstructed τ pair invariant mass distribution for a SM $M_H = 120$ GeV signal and backgrounds after the cuts of Eqs. (7)-(15),(18) and multiplication of the Monte Carlo results by the expected particle ID efficiencies and minijet veto survival probabilities. The double-peaked solid line represents the sum of the signal and all backgrounds. Individual components are: the Hjj signal (solid), the irreducible QCD Zjj background (dashed), the irreducible EW Zjj background (dotted), and the combined reducible backgrounds from QCD + EW + Higgs $WWjj$ events and $t\bar{t} + jets$ and $b\bar{b}jj$ production (dash-dotted).

a complex signal, with a multitude of characteristics which distinguish it from the various backgrounds.

The basic feature of the $qq \to qqH$ signal is the presence of two forward tagging jets inside the acceptance region of the LHC detectors, of sizable p_T, and of dijet invariant mass in the TeV range. Typical QCD backgrounds, with isolated charged leptons and two hard jets, are much softer. In addition, the QCD backgrounds are dominated by W bremsstrahlung off forward scattered quarks, which give typically higher-rapidity charged leptons. In contrast, the EW processes give rise to quite central leptons, and this includes not only the Higgs signal but also EW $WWjj$ and $\tau\tau jj$ production, which also proceed via weak boson fusion. It is this similarity that prevents one from ignoring EW analogs to background QCD processes, which a priori are smaller by two orders of magnitude in total cross section, but after basic cuts remain the same size as their QCD counterparts.

In addition to various invariant mass and angular cuts, one can discriminate between the real τ's of the signal (and of the QCD and EW $\tau\tau jj$ backgrounds) and "fake" τ's from the W, t, b backgrounds. This is possible because the high energy of the produced τ's makes their decay products almost collinear. Combined with the substantial p_T of the $\tau^+\tau^-$ system this allows for τ-pair mass reconstruction. The W decays do not exhibit this collinearity due to their modest boost in the lab frame. This leads to markedly different angular correlations between the $\not{p}_T$ vector and the charged lepton momenta. Our real-τ criteria make use of these differences and largely eliminate the non-τ backgrounds.

We advocate taking advantage of an additional fundamental characteristic of QCD and EW processes. Color-singlet exchange in the t-channel, as encountered in Higgs boson production by weak boson fusion (and in the EW Zjj background), leads to additional soft jet activity which differs strikingly from that expected for the QCD backgrounds in both geometry and hardness: gluon radiation in

QCD processes is typically both harder and more central than in WBF processes. We exploit this radiation, via a veto on events with central minijets of $p_T > 20$ GeV, and expect a typical 70% reduction in QCD backgrounds and about a 25% suppression of EW backgrounds, but only about a 10% loss of the signal.

We have identified the most important distributions for enhancing the signal relative to the background, and set the various cuts conservatively to avoid bias for a certain Higgs boson mass range. There is ample room for improvement of our results. A multivariate analysis of a complete set of signal and background distributions is expected to lead to improved background suppression. Mass specific cuts should eventually be employed and will improve matters as is evident from, e.g., the angular and lepton invariant mass distributions of Figs. 5,6. Additional suppression of the $t\bar{t} + jets$ background may be possible with b identification and veto in the $p_{T_b} < 20$ GeV region. We do not pursue these questions here. One reason is that our results are derived at the parton level only. Even though we have included expected detector resolution effects and losses due to finite trigger and detection efficiencies, a more complete detector simulation is now needed. We have to leave this work to our experimental colleagues.

The very promising results of this study suggest that the $H \to \tau\tau \to ee, \mu\mu + \not{p}_T$ modes should also be considered. The dilepton invariant mass distribution of Fig. 6 shows that elimination of the Z peak in $Z \to ee, \mu\mu$ backgrounds would reduce the Higgs signal by a small amount only. In addition, the requirement of significant $\not{p}_T$ (Eq. (12)) is expected to largely eliminate QCD or EW Zjj production, leaving $ZZjj$ and $ZWjj$ events with invisible Z or W decays as the additional backgrounds. Given our results for the analogous $WWjj$ events we expect these new backgrounds to be minimal. This implies that the purely leptonic $H \to \tau\tau$ signal can most likely be enhanced by almost another factor of two, further reducing the integrated luminosity required for observation of the $H \to \tau\tau$ signal.

Measuring the Higgs-fermion coupling will be an important test of the Standard Model as well as its supersymmetric extension. For such a measurement, via the analysis outlined in this paper, minijet veto probabilities must be precisely known. For calibration purposes, one can analyze Zjj events at the LHC. The production rates of the QCD and EW Zjj events can be reliably predicted and, thus, the observation of the $Z \to \ell\ell$ peak allows for a direct experimental assessment of the minijet veto efficiencies, in a kinematic configuration very similar to the Higgs signal.

In Summary: Observation of the SM or MSSM Higgs scalar(s) via $h/H \to \tau\tau \to e^{\pm}\mu^{\mp}\not{p}_T$ in weak boson fusion is possible at the LHC with modest integrated luminosities, if the Higgs boson lies in the mass range between about 100 and 140 GeV. Extending the search range upward to 150 GeV should eventually be possible. Weak boson fusion at the LHC promises to be an exciting and important channel, both for validating the Standard Model via direct measurement of a Higgs-fermion coupling and as a low-luminosity "see-or-die" test of the MSSM.

ACKNOWLEDGMENTS

We would like to thank R. Kinnunen, A. Nikitenko, E. Richter-Wąs and W. Smith for providing information on expected LHC detector performance. This research was supported in part by the University of Wisconsin Research Committee with funds granted by the Wisconsin Alumni Research Foundation and in part by the U. S. Department of Energy under Contract No. DE-FG02-95ER40896. Fermilab is operated by URA under DOE contract No. DE-AC02-76CH03000.

REFERENCES

[1] For recent reviews, see e.g. J.L. Rosner, Comments Nucl. Part. Phys. **22**, 205 (1998); K.Hagiwara, Ann. Rev. Nucl. Part. Sci. 1998, 463; W.J. Marciano, [hep-ph/9902332]; and references therein.

[2] For recent reviews, see e.g. S. Dawson, [hep-ph/9703387]; M. Spira, Fortsch. Phys. **46**, 203 (1998); and references therein.

[3] W. J. Marciano and F. E. Paige, Phys. Rev. Lett. **66**, 2433 (1991); J. F. Gunion, Phys. Lett. **B261**, 510 (1991).

[4] A. Stange, W. Marciano, and S. Willenbrock, Phys. Rev. **D50**, 4491 (1994); R. Kleiss, Z. Kunszt, W. J. Stirling, Phys. Lett. **B253**, 269 (1991); H. Baer, B. Bailey, J. F. Owens, Phys. Rev. **D47**, 2730 (1993).

[5] ATLAS Collaboration, Technical Design Report, report CERN/LHCC/99-15 (1999); G. L. Bayatian *et al.*, CMS Technical Proposal, report CERN/LHCC/94-38 (1994).

[6] D. Rainwater and D. Zeppenfeld, Phys. Rev. **D60**, 113004 (1999) [hep-ph/9906218].

[7] D. Rainwater, PhD thesis, hep-ph/9908378.

[8] M. Dittmar and H. Dreiner, Phys. Rev. **D55**, 167 (1997); and [hep-ph/9703401].

[9] H. E. Haber and R. Hempfling, Phys. Lett. **D48**, 4280 (1993); M. Carena, J.R. Espinosa, M. Quiros, and C.E.M. Wagner, Phys. Lett. **B355**, 209 (1995).

[10] S. Heinemeyer, W. Hollik and G. Weiglein, Phys. Rev. **D58**, 091701 (1998); R.-J. Zhang, Phys. Lett. **B447**, 89 (1999).

[11] R. N. Cahn, S. D. Ellis, R. Kleiss and W. J. Stirling, Phys. Rev. **D35**, 1626 (1987); V. Barger, T. Han, and R. J. N. Phillips, Phys. Rev. **D37**, 2005 (1988); R. Kleiss and W. J. Stirling, Phys. Lett. **200B**, 193 (1988); D. Froideveaux, in *Proceedings of the ECFA Large Hadron Collider Workshop*, Aachen, Germany, 1990, edited by G. Jarlskog and D. Rein (CERN report 90-10, Geneva, Switzerland, 1990), Vol II, p. 444; M. H. Seymour, *ibid*, p. 557; U. Baur and E. W. N. Glover, Nucl. Phys. **B347**, 12 (1990); Phys. Lett. **B252**, 683 (1990).

[12] V. Barger, K. Cheung, T. Han, and R. J. N. Phillips, Phys. Rev. **D42**, 3052 (1990); V. Barger *et al.*, Phys. Rev. **D44**, 1426 (1991); V. Barger, K. Cheung, T. Han, and D. Zeppenfeld, Phys. Rev. **D44**, 2701 (1991); erratum Phys. Rev. **D48**, 5444 (1993); Phys. Rev. **D48**, 5433 (1993); V. Barger *et al.*, Phys. Rev. **D46**, 2028 (1992).

[13] D. Dicus, J. F. Gunion, and R. Vega, Phys. Lett. **B258**, 475 (1991); D. Dicus, J. F. Gunion, L. H. Orr, and R. Vega, Nucl. Phys. **B377**, 31 (1991).

[14] Y. L. Dokshitzer, V. A. Khoze, and S. Troian, in *Proceedings of the 6th International Conference on Physics in Collisions*, (1986) ed. M. Derrick (World Scientific, 1987) p.365; J. D. Bjorken, Int. J. Mod. Phys. **A7**, 4189 (1992); Phys. Rev. **D47**, 101 (1993).

[15] V. Barger, R. J. N. Phillips, and D. Zeppenfeld, Phys. Lett. **B346**, 106 (1995).

[16] D. Rainwater, D. Zeppenfeld and K. Hagiwara, Phys. Rev. **D59**, 014037 (1999).

[17] T. Plehn, D. Rainwater and D. Zeppenfeld, Phys. Lett. **B454**, 297 (1999).

[18] H. L. Lai *et al.*, Phys. Rev. **D55**, 1280 (1997).

[19] R. Cahn and S. Dawson, Phys. Lett. **136B**, 196 (1984).

[20] D. Rainwater and D. Zeppenfeld, Journal of High Energy Physics 12, 005 (1997).

[21] D. Rainwater, R. Szalapski, and D. Zeppenfeld, Phys. Rev. **D54**, 6680 (1996).

[22] T. Stelzer and W. F. Long, Comp. Phys. Comm. **81**, 357 (1994).

[23] A. Stange, private communication.

[24] D. Zeppenfeld, preprint MADPH-99-1143.

[25] D. Cavalli, L. Cozzi, L. Perini, S. Resconi, ATLAS Internal Note PHYS-NO-051, Dec. 1994.

[26] S. D. Ellis, R. Kleiss, and W. J. Stirling, Phys. Lett. **154B**, 435 (1985); R. Kleiss and W. J. Stirling, Nucl. Phys. **B262**, 235 (1985); Phys. Lett. **180B**, 171 (1986); J. F. Gunion, Z. Kunszt, and M. Soldate, Phys. Lett. **163B**, 389 (1985); Erratum, Phys. Lett. **168B**, 427

(1986); J. F. Gunion and M. Soldate, Phys. Rev. **D34**, 826 (1986); R. K. Ellis and R. J. Gonsalves, in *Proc. of the Workshop on super high energy physics*, Eugene, OR (1985), ed. D. E. Soper, p. 287.

[27] V. Barger, T. Han and J. Ohnemus, and D. Zeppenfeld, Phys. Rev. Lett. **62**, 1971 (1989); Phys. Rev. **D40**, 2888 (1989).

[28] H. Chehime and D. Zeppenfeld, Phys. Rev. **D47**, 3898 (1993).

[29] V. Barger, T. Han, J. Ohnemus and D. Zeppenfeld, Phys. Rev. **D41**, 2782 (1990).

[30] R. K. Ellis *et al.*, Nucl. Phys. **B297**, 221 (1988).

[31] S. Nikitenko, E. Richter-Wąs, private communication.

[32] A. Duff and D. Zeppenfeld, Phys. Rev. **D50**, 3204 (1994); K. Iordanidis and D. Zeppenfeld, Phys. Rev. **D57**, 3072 (1998).

[33] V. Barger and R. J. N. Phillips, Phys. Rev. Lett. **55**, 2752 (1985); H. Baer, V. Barger, H. Goldberg, and R. J. N. Phillips, Phys. Rev. **D37**, 3152 (1988).

[34] D. Rainwater, D. Summers, and D. Zeppenfeld, Phys. Rev. **D55**, 5681 (1997).

[35] A. Djouadi, J. Kalinowski, and M. Spira, Comput. Phys. Commun. **108**, 56 (1998).

[36] J. Conway, H. Haber, J. Hobbs and H. Prosper, "Statistical Conventions and Method for Combining Channels for the Tevatron Run 2 SUSY/Higgs Workshop Higgs Working Group", Report v5, 1999.

[37] See Talks by the LEP Collaborations, LEPC 11/9/99.